Australian Government
Department of Defence
Defence Science and
Technology Organisation

Design Methodology for Bonded Repair to Partial Through-Thickness Damage

Chun Hui Wang and Dina Pilalis

Air Vehicles Division
Defence Science and Technology Organisation

DSTO-TR-2117

ABSTRACT

Partial through-thickness damage to metallic and composite structures, like those caused by corrosion damage of metals or foreign object impact to composites, can be repaired by adhesively bonding an insert and an external doubler. The design methodology for these types of repairs is based on a simplified analysis in which the insert is assumed to be bonded to the flat bottom of the cutout area. This report presents an investigation of the accuracy and limitations of the curent design methodology using the finite element method. Improved design methods are also presented, including the optimum taper angle of the grindout and the required overlap length. Validity of the design methodology was assessed by comparison with experimental testing of repairs tapered at different angles.

Published by

Air Vehicles Division
DSTO Defence Science and Technology Organisation
506 Lorimer St
Fishermans Bend, Victoria 3207 Australia

Telephone: (03) 9626 7000
Fax: (03) 9626 7999

AR-014-166
September 2008

APPROVED FOR PUBLIC RELEASE

Design Methodology for Bonded Repair to Partial Through-Thickness Damage

Executive Summary

Partial through-thickness damage, such as corrosion damage to metallic structures and impact damage to composite structures, is a common type of structural defect requiring repairs to restore structural integrity to aircraft. After removing the damaged material, a tapered plug and/or an external doubler is adhesively bonded. The design procedure for these types of repairs is prescribed in the Royal Australian Air Force's Engineering and Design Procedures for Composite and Adhesive Bonded Repairs (AAP 7021.016-1). Recently the issuing authority of the RAAF standard requested DSTO to undertake a verification and validation investigation of the recommended methodology as described in the standard. This report presents the technical approach and results of the substantiation study.

The various design parameters, including the scarfing angle of damage cutout, the tapering ratio and edge height of doubler, and the depth of insert are investigated using the finite element method. The numerical results are compared to the analytical solutions in accordance with the approved design procedure. The results revealed that the current recommended scarf angle of 30 degrees is only valid for structures designed to relatively low strength levels, because of the limited shear strength of existing structural adhesives. A smaller scarf angle, which can be determined from the numerical results for desired repair strengths, is necessary to avoid premature disbonding of the repair plug from the cutout. It is also shown that in the case of thick adherends, the existing design procedure is overly conservative. A shear-lag correction has been found to provide a simple means of reducing the level of conservatism. Finally, a revised solution of the overlap length has also been developed to take into account the load-carrying capacity of the unbroken ligament, which can significantly reduce the size and repair and hence increase the applicability of bonded repairs to structures with limited edge distance.

This investigation has shown that the current design procedures prescribed in the RAAF Engineering Standard are satisfactory for relatively thin structures carrying relatively low stress. For moderately thick structures designed to operate at high stress levels, a shear-lag correction is needed to reduce the level of conservatism of existing design. New design methodologies have also been developed and numerically shown to offer considerable improvement to repair design. It is recommended to incorporate the new methodology in the next revision of the RAAF Design Standard.

Authors

Chun Hui Wang
Air Vehicles Division

Chun Wang is the Head of the Advanced Composite Technologies group in the Air Vehicles Division. His main research expertise is in the areas of solid mechanics, including fatigue and fracture mechanics, dynamics, composite structures, joining and repair technologies, and scattering of acoustic and electromagnetic waves.

Dina Pilalis
QinetiQ AeroStructures

Dina Pilalis graduated from RMIT University in 2003 with a degrees in Aerospace Engineering (honours). She is currently working for QinetiQ Aerostructures and is contracted to the Air Vehicles Division at DSTO since 2005, working predominantly in finite element analysis, and research.

Contents

1. Introduction

Some frequently encountered defects that need structural repairs for strength restoration include corrosion damage to metallic structures and surface impact damage to composite structures. Repair to corrosion damage involves the removal and blending out of the corrosion together with the use of a filler and an externally bonded doubler. Similarly, part-through damage in composites can be repaired by removing the damaged material and then bonding an insert and external doubler. The current design approach for these types of structural repairs is described in an engineering standard [1], which has been revised recently to incorporate improved solutions of thermal residual stresses [2, 3] resulting from cure and in-service temperature excursions.

The design procedures described in the engineering standard [1] have been developed by treating the representative bonded joint as beams connected by distributed springs. Previous studies [2, 3] have confirmed that the beam-spring model can accurately describe the stresses along the mid-plane of the adhesive in repairs to through-thickness damages. The purpose of this report is to present a numerical investigation to verify the design methodology for single-sided repair to a part-through thickness defect as outlined in Appendix 3 to Annex C, Chapter 6 of AAP 7021.016-1 [4].

Structural defects are caused either by in-service degradation (corrosion or foreign object impact), or design inadequacies. In the latter case, repairs need to be stronger than the original design strength. In both cases, the major concern of repair design is to ensure that the adhesive bond strength exceeds the required design strength with a sufficient margin. The major emphasis of this report is to assess the calculated peak adhesive stresses against the numerical values determined using the finite element method. A description of the problem is given in Section 2, with the FE model employed in the study presented in Section 3. In Section 4, the numerical results from the FE analysis are compared to analytical solutions. To improve the accuracy of the analytical solutions for thick adherends, a shear-lag correction term, summarised in Section 5, has been included in the present study. Finally the required overlap length that accounts for the load-carrying capacity of the unbroken ligament is given in Section 6.

2. Problem Description

A one-sided repair to a partial through-thickness defect is shown in Figure 1, indicating the variables considered in the design analysis. The depth and length of the part-through cutout are respectively denoted as t_i^* and $2L_D$. The existing design approach requires that the bottom of the defect is machined essentially flat and the sides of the cutout are scarfed at an angle not exceeding 30 degrees ($\theta \le 30°$) or a taper ratio of 1:1.732. An insert plug made of the same material as the structure is bonded into the cutout prior to the installation of a bonded patch over the insert. The edge of the repair doubler is normally tapered to a ratio of 1:10 to reduce peel and shear stresses [5], which is equivalent to setting $\beta = 5.7°$.

To design against failures in the adhesive bond, the repair doubler, and the original structural member, the maximum stresses in the adhesive, the structural member (including stress concentration resulting from cutout), and the repair (insert and doubler) must be kept below the respective critical values. Expressions for these quantities are provided in Appendix 3 to Annex C, Chapter 6 of AAP 7021.016-1 [4]. It is worth noting that the adhesive shear stress solution in Ref. [4] is very conservative, neglecting the load being transferred by the adhesive bond between the tapered sides of the cutout. Furthermore, the damage size is assumed to be much greater than the thickness of the structural member ($L_D >> t_i$), so that the two peak stresses at the ends of the cutout are uncoupled.

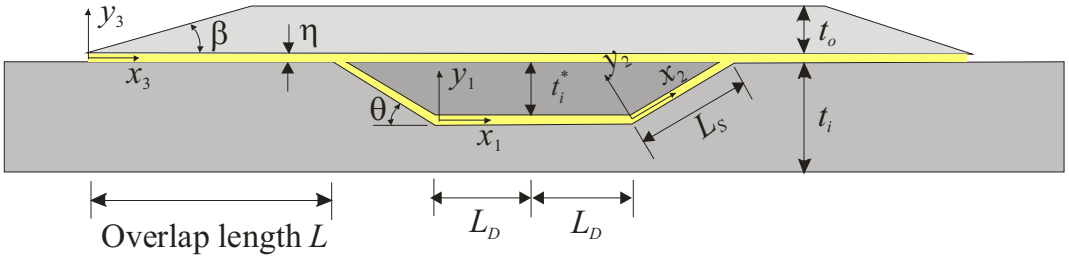

Figure 1: Structural model representing one-sided repair to a part-through defect

3. Analytic Solutions

Given that the repair insert is normally made of the same material as the structural member, the adhesive stresses along the scarf are approximately constant, depending only on the taper angle and the applied load. The average shear and peel stresses are given by [6]

$$\tau = \frac{\sigma_{applied}}{1+S}\sin\theta\cos\theta, \tag{1}$$

$$\sigma_c = \frac{\sigma_{applied}}{1+S}\sin^2\theta, \tag{2}$$

with $S = E_o t_o / E_i t_i$ denoting the stiffness ratio of the repair. It is readily seen that for a scarf angle $\theta = 30°$, the repair can only sustain an applied stress comparable to the shear or peel strength of the adhesive, which is often significantly less than the strength of metallic or composite materials. As an example, consider a structure made of aluminium alloy 7075-T6 alloy, which has a yield stress of 500 MPa. Assuming that the design ultimate strength is approximately equal to the yield stress (corresponding to design limit strength of 333 MPa), the adhesive shear stress pertinent to a half-thickness ($S = 0.5$) cutout tapered at 30 degrees would be 144.3 MPa, far exceeding the highest shear strength of extant structural adhesives (Annex A to Chapter 6 [4]). Therefore, the scarf angle θ must be made smaller to avoid adhesive failure.

In recognition of the propensity of adhesive failure along the sides of 30-degree grindout [7], the current design methodology [4] assumes that the sides of the cutout are not bonded. So

effectively the design treats the cutout as being straight-sided, as illustrated in Figure 2. The maximum adhesive shear strain at location C is given by

$$\gamma_o = \begin{cases} \dfrac{\sigma^*_{insert} t^*_i \lambda}{G}, & \gamma_o \le \gamma_e \\ \dfrac{\tau_p}{2G}\left[1+\left(\dfrac{\sigma^*_{insert} t^*_i \lambda}{\tau_p}\right)^2\right], & \gamma_o > \gamma_e \end{cases} \tag{3}$$

with

$$\lambda^2 = \frac{G}{\eta}\left(\frac{1-\nu_i^2}{E_i t_i} + \frac{1-\nu_o^2}{E_o t_o}\right), \tag{4}$$

$$\sigma^*_{insert} = \frac{E^*_i t_i}{E_o t_o + E^*_i t^*_i + E_i (t_i - t^*_i)} \sigma_{applied}\,. \tag{5}$$

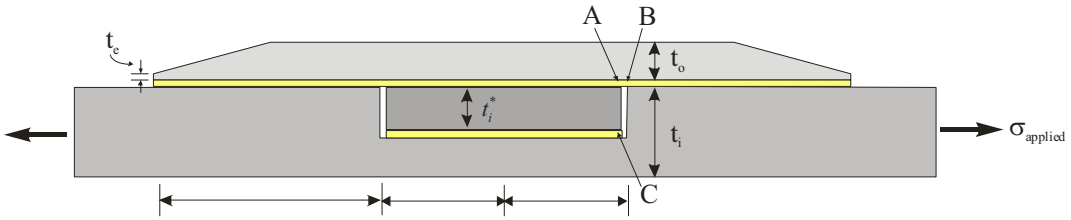

Figure 2: Straight-edge cutout repair

It is worth noting that the adhesive at locations A and B would also experience a similar magnitude of strain concentration. To verify the accuracy and limitations of the design methods [4] as summarised above, FE analyses of representative joints shown in Figure 1 and Figure 2 will be performed for various combinations of scarf angle θ, part-through defect depth t^*_i, and tapering angle β.

In accordance with DEF(AUST) 9005 Chapter 14 [5], the outer edges of the patch are tapered to reduce peel and shear stresses. For composite patches, this is achieved by terminating each ply during lay-up. For metallic patches, the out edges are tapered to a ratio of 1:10, with the tip height ranging between 0.5 and 1.0 mm. The reduction factor of the peel stress relative to a block-end doubler is estimated using the following relationship [4],

$$\frac{(\sigma_{c\max})_{tapered}}{(\sigma_{c\max})_{uniform}} = \sqrt{\frac{3t_e}{t_e + t_o}}\,, \tag{6}$$

where t_e denotes the height of the tip as shown in Figure 2. It is apparent that this expression gives an incorrect value for a uniform (no taper) repair ($t_e = t_o$). In this work the validity of this solution will be also be examined.

4. Finite Element Model

A finite element (FE) analysis was performed to verify the accuracy of the design method for one-sided repairs to structures that contain part-through defects. Both tapered cutout (Figure 1) and straight-sided cutout (Figure 2) were modelled. A doubler is adhesively bonded to cover the repair insert. In the case of a straight-sided cutout, the repair insert is bonded to the structure with adhesive on the lower surface. FE analysis was performed using StressCheck™ under plane-strain conditions.

The repair insert and the repair doubler are assumed to be made of the same material as the structural member. For the purpose of verification, the model material is assumed to have a Young's modulus of 70 GPa and Poisson's ratio of 0.3, representative of aluminium alloy. The adhesive's properties will be varied to examine the influence of shear stiffness on the stress distribution. The parametric FE model, referring to Figure 3, allows the depth of cutout, the scarf angle, the adhesive thickness, and the end tapering angle to be varied, enabling a comprehensive verification of the accuracy and limitation of the design procedures.

4.1 Scarf angle

Six different scarf angles were considered: $3°$, $6°$, $15°$, $30°$, $60°$, and $90°$. The cutout depth is assumed to be 50% of the thickness of the structural member. The analytical solutions (1) and (2) have been derived for a doubler-scarf repair to full thickness damage. The adhesive thickness was varied between 0.01 mm and 0.4 mm to investigate the effect of joint flexibility on adhesive stresses. The analytic expressions (1) and (2) are valid for part-through damage repair with vanishing adhesive thickness.

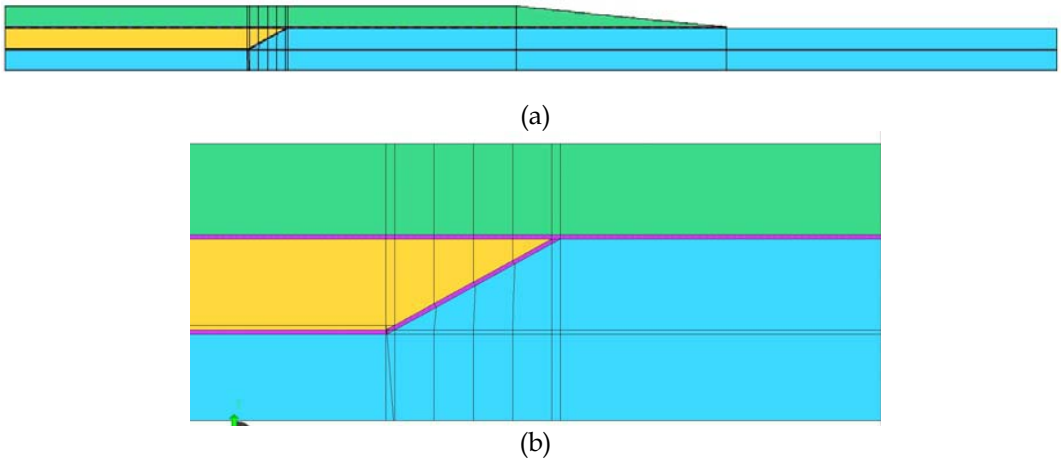

(a)

(b)

Figure 3: Parametric FE model of part-through thickness repair with varying scarf angle; (a) full model, (b) mesh near scarf region.

4.2 Straight-edge cutout

The current design analysis for bond strength is based on the conservative assumption that the insert is not bonded to the scarf sides of the cutout. To verify the analytical solution, the depth of the cutout is varied between 10% and 70% of the thickness of the structural member, with the sides of the cutout being perpendicular to the bondline ($\theta = 90°$).The doubler and the insert are always equal in thickness. The length of the panel was given by the length of the doubler plus an additional length to isolate edge effect. The insert dimensions were varied when investigating the effect of the taper angle of the insert.

Representative joint structure was modelled using two-dimensional plane-strain elements. Symmetry conditions and boundary constraints are indicated in Figure 4.

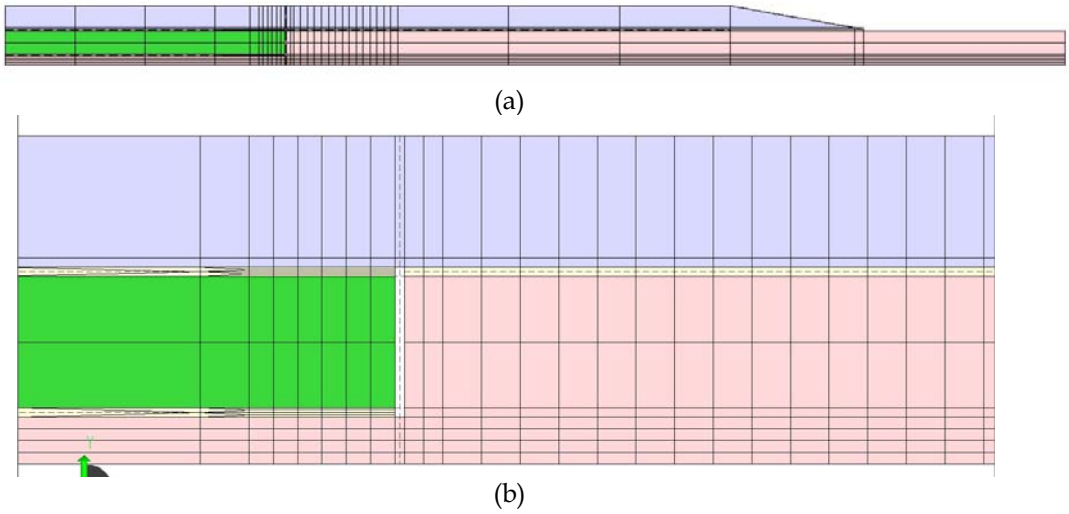

Figure 4: FE model of part-through damage repair; (a) a half- model and (b) mesh near cutout

4.3 Patch end tapering

The patch is tapered at a ratio of 1:10, in accordance with the current design standard [5]. Denoting the thickness of the repair as t_o and the edge height as t_e, the length of the tapered region is equal to $10(t_o - t_e)$. An example of the FE model is shown in Figure 5, in which the edge height t_e can be varied. A triangular fillet is assumed to exist at the edge of the repair. Due to the existence of a corner singularity at the adhesive-repair interface, adhesive shear and peel stresses will be extracted along the mid-plane of the adhesive layer. The material properties and dimensions of the parent and repair are listed in Table 1. Various edge heights are considered, ranging between 10% and 50% of the full repair thickness.

Table 1: Material properties and dimensions employed in study of patch end tapering (unless otherwise stated on figure)

Parameters	Parent	Repair	Adhesive
Young's modulus	70 GPa	70 GPa	2600 MPa
Poisson's ratio	0.3	0.3	0.3
Thickness	3 mm	3 mm	0.15 mm

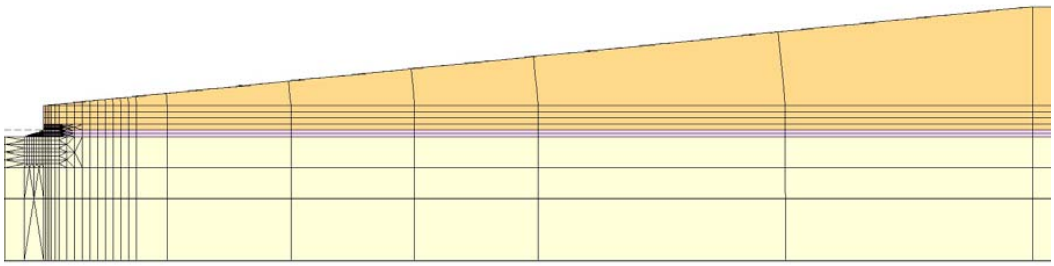

(a) FE model for a tapered repair

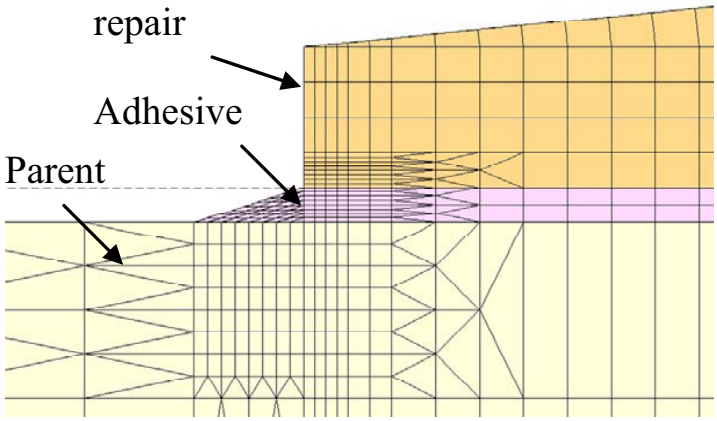

(b) Fine mesh near edge of repair

Figure 5: FE model of tapered doubler

5. Comparison between analytical solution and FE results

5.1 Model Convergence

One advantage of StressCheck™ is its high order polynomial element formulation (*p*-element), which allows the use of coarser meshes with element aspect ratio being as high as 200:1. By contrast, the conventional h-version finite elements are limited to aspect ratio of up to 10:1. The very large length to thickness ratio of bonded joints makes the *p*-version of StressCheck particularly advantageous. To confirm the accuracy of the present FE model, a convergence study was carried out. Figure 6(a) shows a coarse mesh, where the adherends near the cutout

are modelled with only a few elements. A more refined mesh of the model is shown in Figure 6(b).

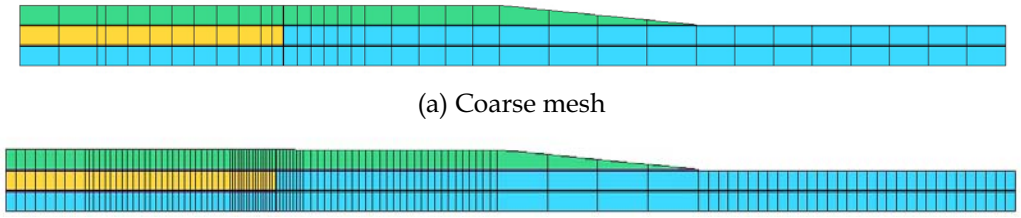

(a) Coarse mesh

(b) Fine mesh

Figure 6: FE meshes for convergence study

Results of the normalised adhesive shear stress along the bondline between the parent and the filler, which is 50% of the thickness of the parent structure, are displayed in Figure 7. The parent structure is 6.35mm in thickness. It is seen that as the FE mesh density was doubled, the peak shear stress increased from 0.208 to 0.209, suggesting that the accuracy of the fine mesh model is better than 0.5%. In the following analyses, the refined mesh will be employed.

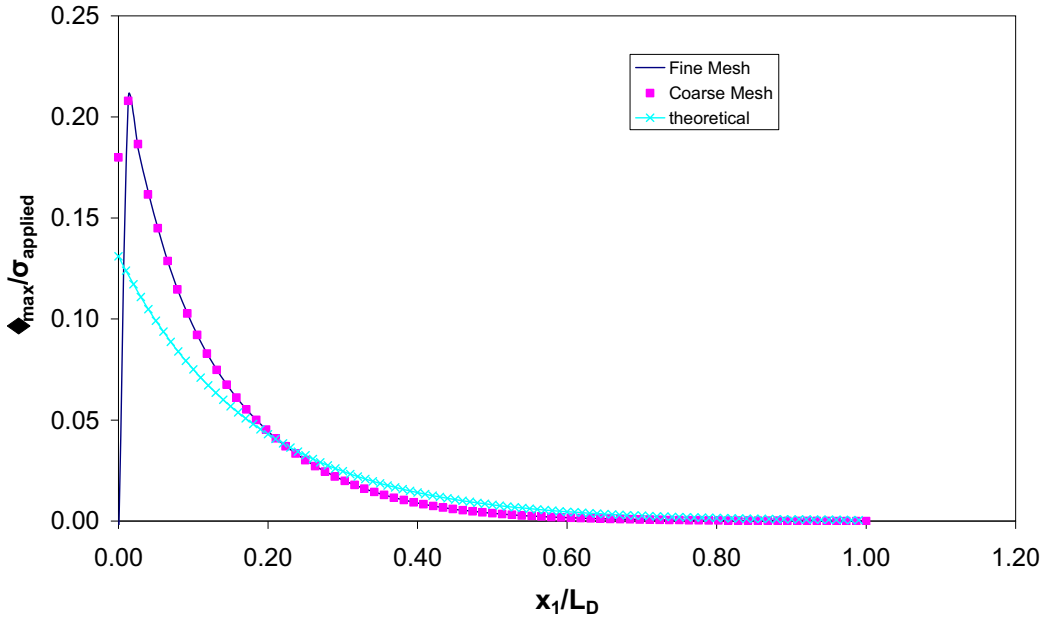

Figure 7: Verification of convergence (applied stress=1.0, η=0.15mm)

5.2 Influence of scarf angle

Six different scarf angles were investigated, including 3°, 6°, 15°, 30°, 60° and 90°. The cutout depth was kept constant at 50% of the thickness of the structural member. The shear stress and peel stress were taken in a local coordinate system along the midline of the adhesive

bond, as shown in Figure 1. The results are shown in Figure 8 together with the results from the analytical expression (1). It is seen that in all cases the adhesive shear stress attains its peak value in the interior rather than at the ends, as in the case of overlap joint. Also shown in Figure 8 is the analytical solution of the maximum adhesive shear stress. As the taper angle increases, the analytical solution deviates further from the FE results, due to the shear lag effect that prevents the full development of the shear stress along the tapered sides. If the adhesive thickness is reduced to close to zero, the adhesive shear stress would approach the analytic solution, as shown in Figure 9(a).

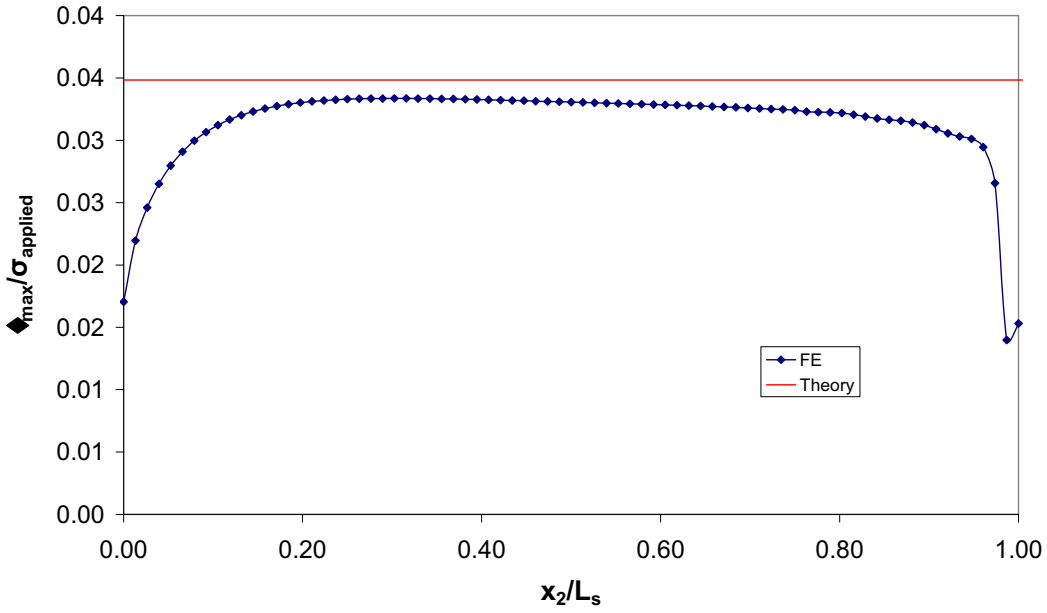

(a) 3-degrees

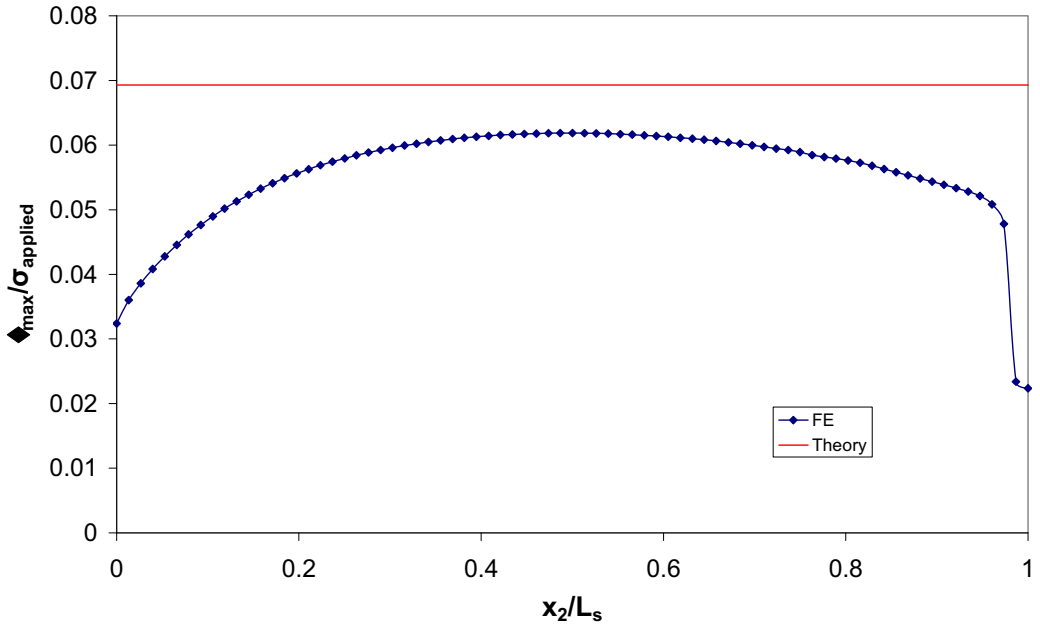

(b) 6-degrees

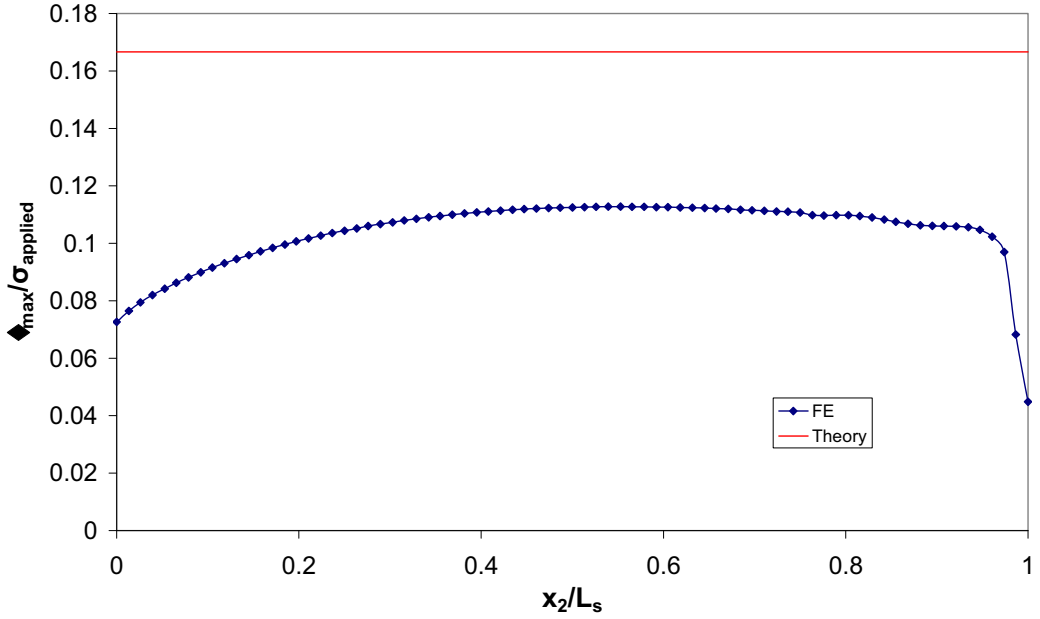

(c) 15-degrees

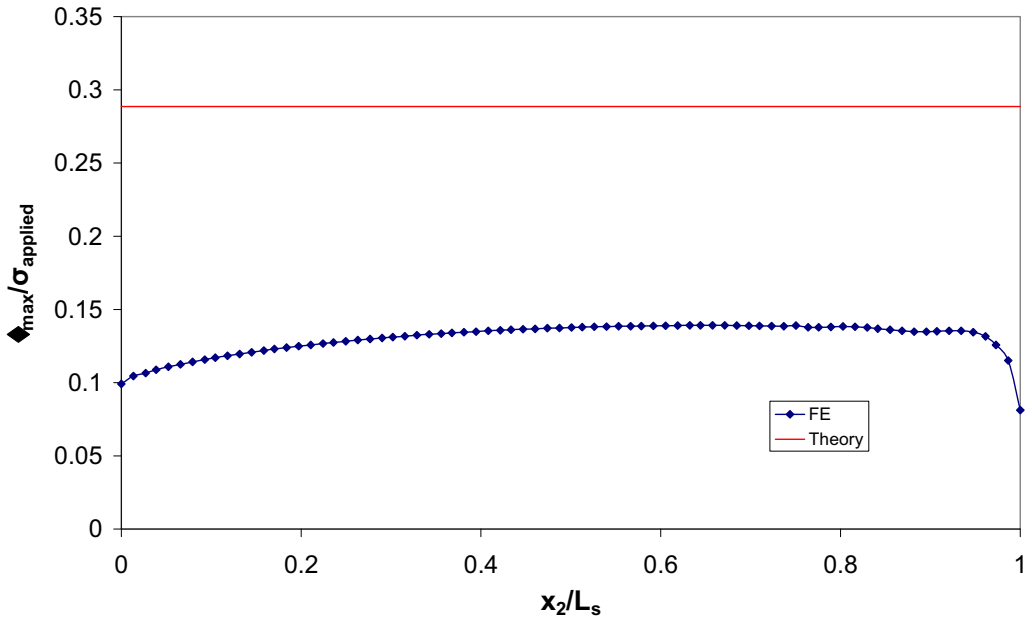

(d) 30-degrees

Figure 8: Shear stress for (a) 3-degree (b) 6-degree (c) 15-degree (d) 30-degree scarf insert to a 50% part-through thickness defect ($t_i^* = 0.5t_i$, $\eta = 0.15$ mm)

The low magnitude of adhesive shear stress shown in Figure 8 indicates that a three-degree scarf insert would be able to achieve high repair strength. The shallow scarf angle, however, requires the removal of a large amount of undamaged material. The necessary material removal can be reduced by using a higher scarf angle, provided the adhesive bond is not overly stressed. According to Equations (1) and (2), both adhesive shear and peel stresses in through-thickness repair increase rapidly with scarf angle, so it is necessary to confirm whether a part-through thickness scarf insert would experience the same level of stresses. Presented in Figure 9 is the variation of adhesive stresses versus scarf angle for four adhesive thicknesses. For a very thin adhesive bond, the FE results agree well with the analytical solution (1), which is expected as the analytical solutions are derived on the assumption of the adhesive being vanishingly small. For higher scarf angles, thicker bond results in lower adhesive stresses, with the reduction in shear stress being greater than the percentage reduction in peel stress.

To avoid premature failure of the adhesive bond, the shear and peel stresses need to be kept below the respective critical values for a given structural adhesive. Based on the finite element results shown in Figure 9(a), a conservative estimate of the ultimate repair strengths (defect depth is 50% of the structure thickness) with FM300-2 adhesive for different scarf angles are shown in Figure 11. Here the adhesive bond is considered to attain its full strength when the peak shear stress reaches the maximum allowable shear stress, effectively neglecting the extra load carrying capacity of adhesive undergoing plastic deformation.

For structures designed to operate at higher stress, it is necessary to reduce the taper angle to insure adhesive bond remains intact. The appropriate angle can be determined from the results shown in Figure 9.

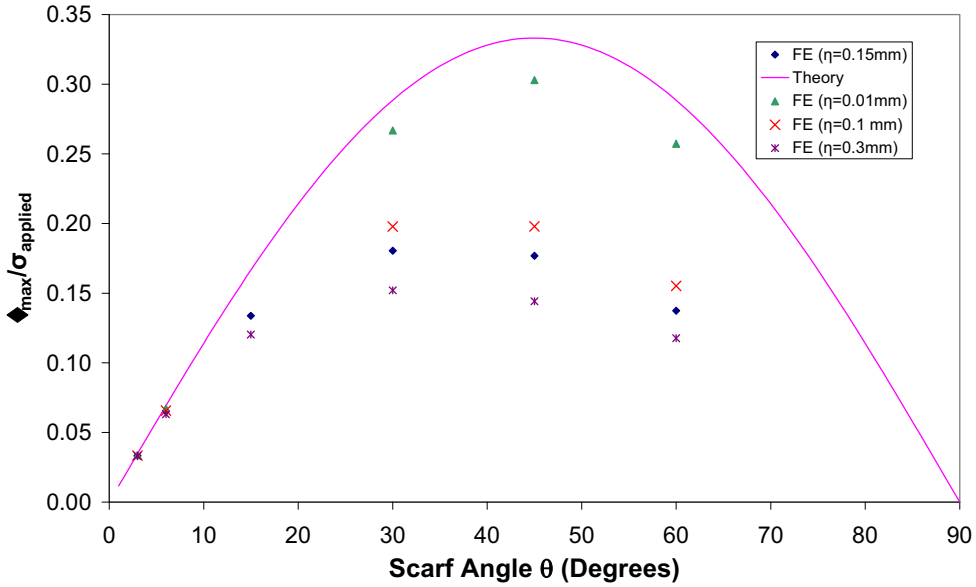

(a)

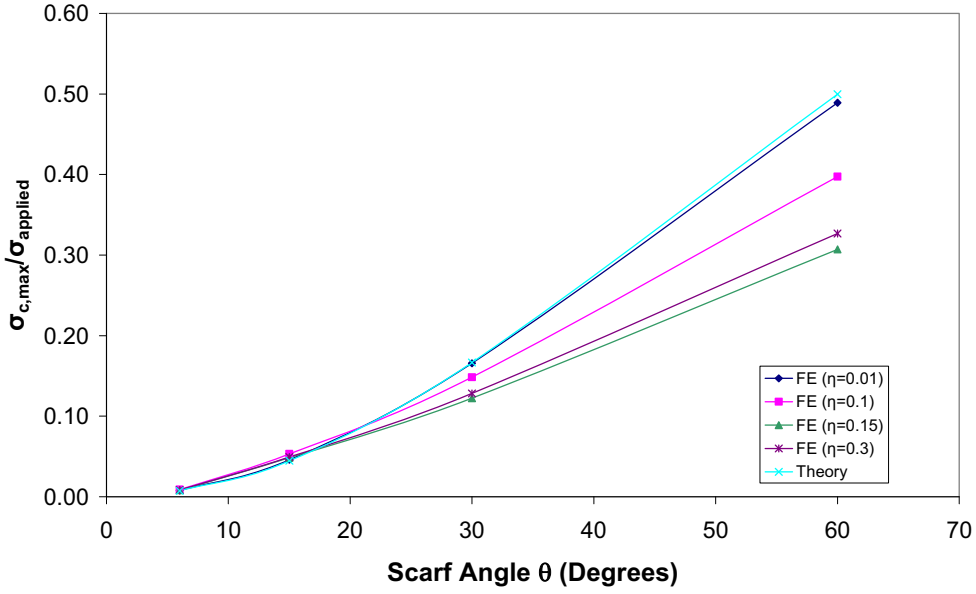

(b)

Figure 9: Comparison of finite element results with analytical solution; (a) adhesive shear stress and (b) adhesive peel stress. Cutout depth is 50% of the structure thickness ($t_i^* / t_i = 0.5$). Note Young's modulus used for the adhesive is 1248 MPa.

Since structural adhesives can sustain a considerable amount of plastic deformation in shear prior to failure, the aforementioned elastic analyses can underestimate the bond strength. To quantify the effect of adhesive plastic deformation on repair strength, an elastic-plastic analysis was carried out using FE in which the adhesive is allowed to undergo plastic deformation. The adhesive was modelled as perfectly plastic. The properties of FM300-2 adhesive at 88°C/saturation were employed. Specifically, the shear modulus of the adhesive was 200 MPa, with a Poisson's ratio of 0.3 and a shear yield stress of 23.3 MPa. Results of the peak adhesive shear strain are presented in Figure 10 for three different tapering angles. Given that FM300-2 adhesive can reach a total shear strain of 0.325 at 88°C with full moisture saturation, the highest strength that can be attained by the bonded filler-doubler repair may exceed the estimated strength based on elastic analysis. Using the results displayed in Figure 10, the repair strength for a given taper angle can be calculated. The results are shown in Figure 11, from which the necessary taper angle required to achieve a given repair strength can be determined. For example, if the sides of the cutout are tapered at 30 degrees, the damaged component can be restored to strength of 300 MPa. However, if the taper angle can be lowered to 6 degrees, the repair strength can reach 550 MPa.

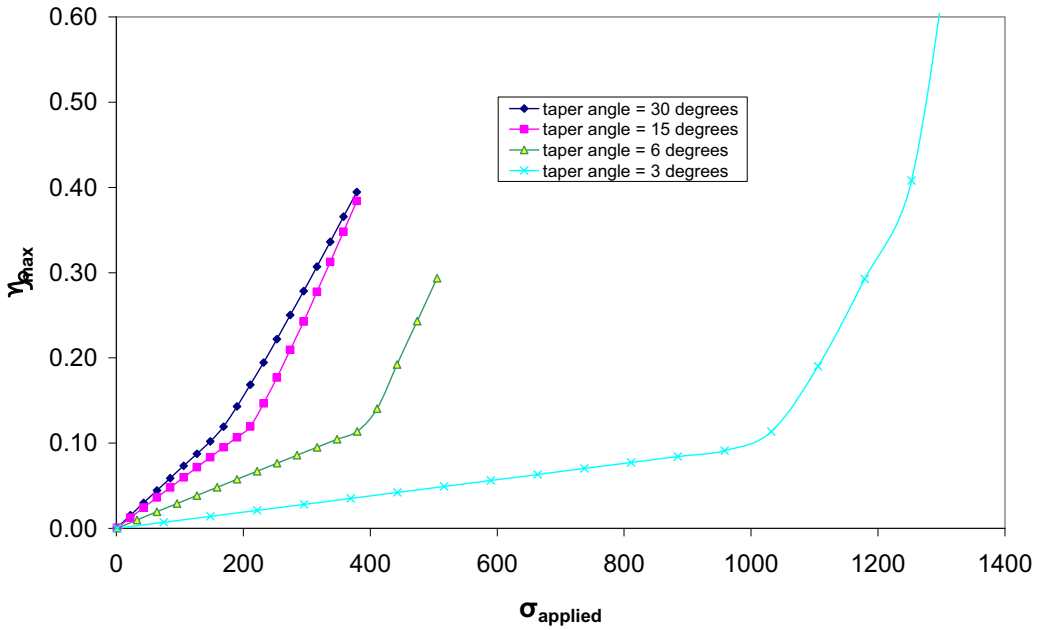

Figure 10: Maximum adhesive shear strain along a tapered side of cutout. The depth of the cutout is 50% of the thickness of the parent structure.

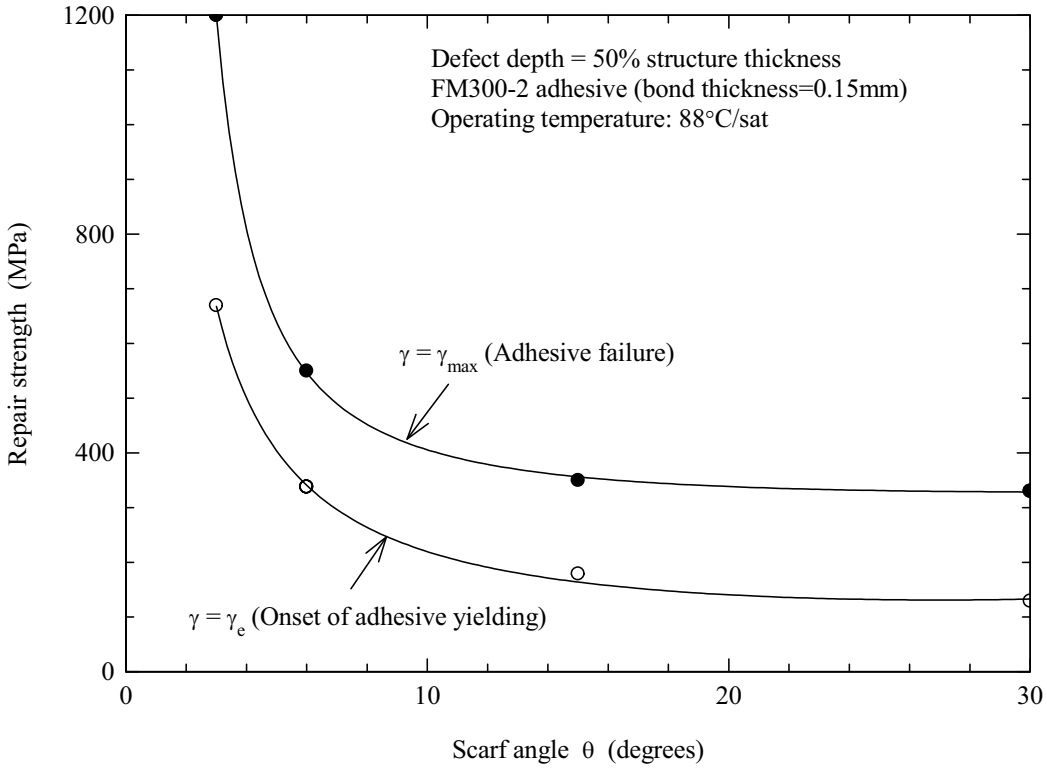

Figure 11: Ultimate bond strength (shear failure) versus scarf angle (defect depth is 50% of the structural thickness). Peel failure is not considered.

5.3 Cutout depth

Due to the presence of the gap between the sides of the insert and the sides of the cutout, as illustrated in Figure 2, the adhesive between the doubler and parent structure, location A and location B, also experiences high stress concentrations. The results shown in Figure 12 indicate that the maximum shear stress occurs at point C, consistent with the assumption made in [4]. As a result, stresses around point C will be used in further verifications.

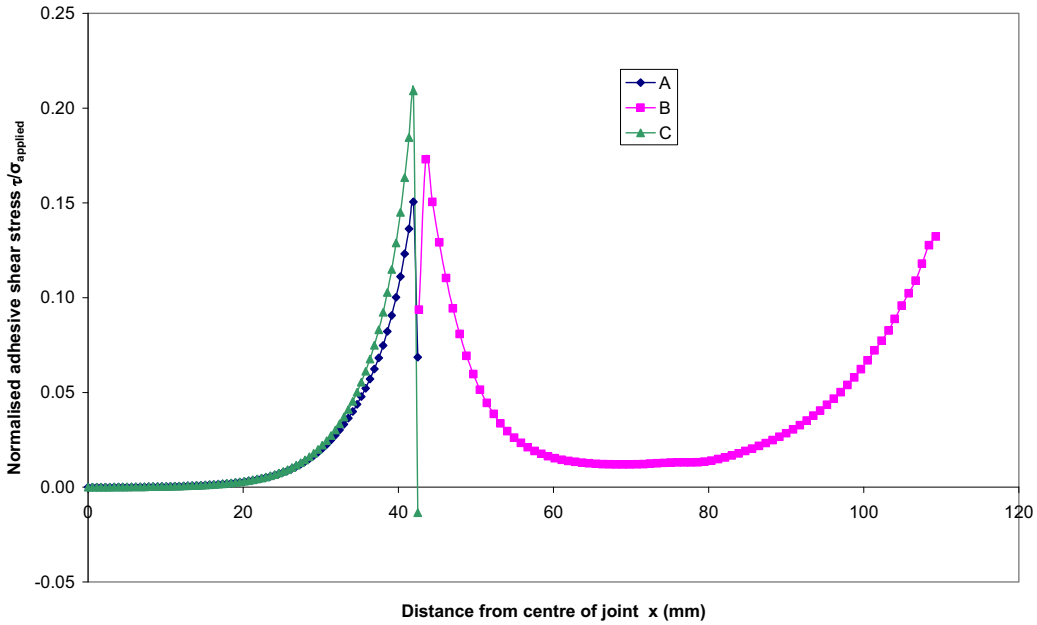

Figure 12: Shear strain distributions around cutout

To verify the accuracy of the current design approach, elastic FE analyses were first carried out using the model shown in Figure 4, for two different adherend thicknesses: 3.0 mm and 1.0 mm. Results of the elastic adhesive shear stress at the insert-cutout boundary are presented in Figure 13.

The effect of cutout depth on peak adhesive shear stress is clearly seen in Figure 14. For structures under 1.0 mm thickness the existing solutions overestimate the peak shear stress by about 20%. However, for structures with a thickness of 3.0 mm, the analytical solution overestimates by between 30% and 40%, which represents a considerable level of conservatism that may limit the applicability of bonded repairs. An improvement can be achieved by including the effect of shear lag, which will be discussed in Section 6.

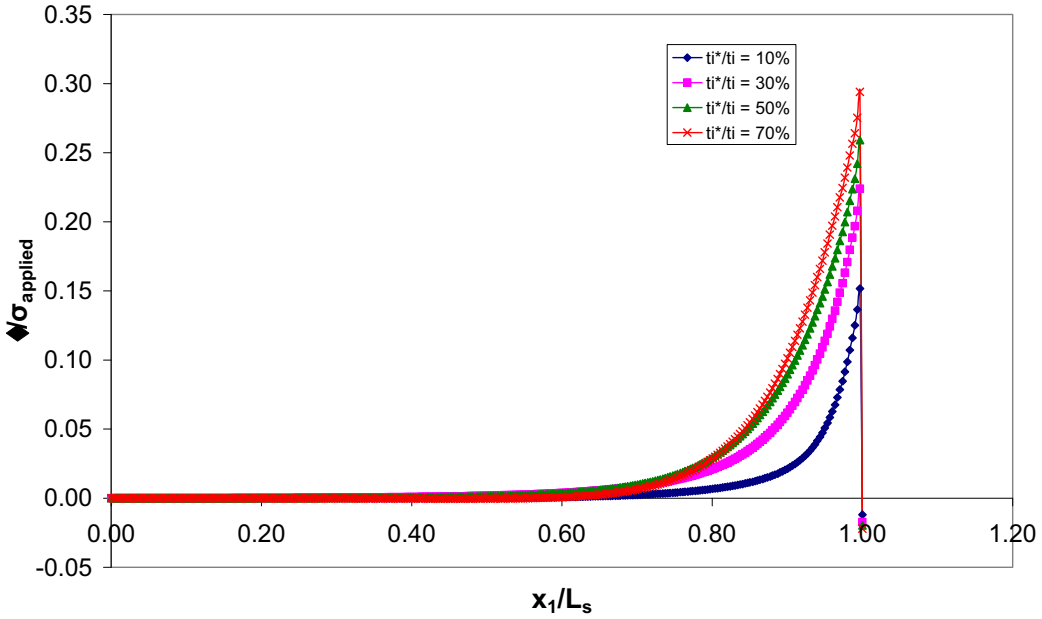

(a)

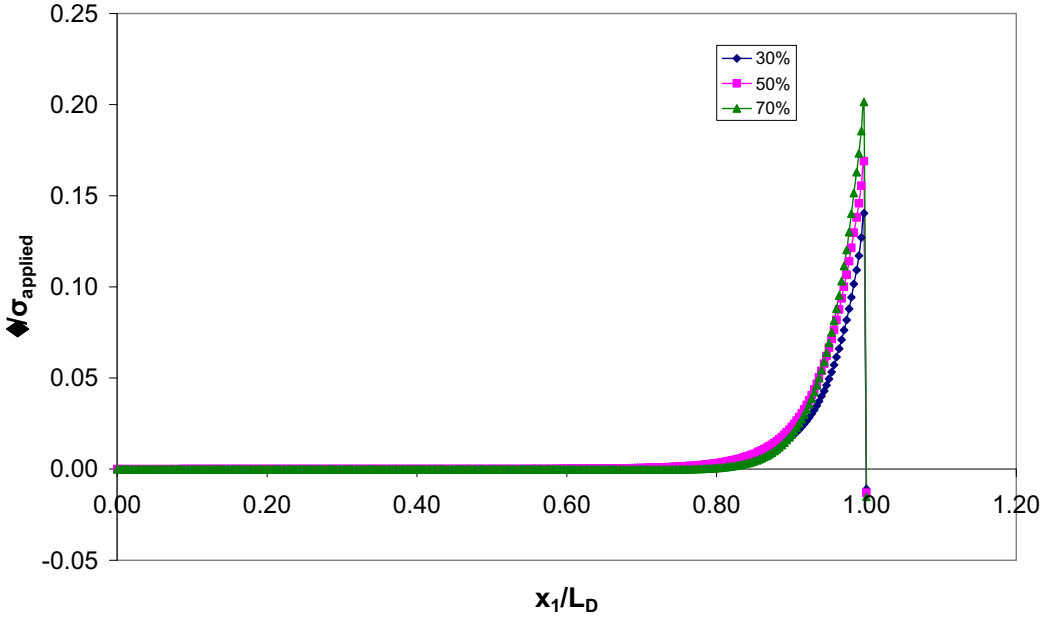

(b)

Figure 13: Distributions of shear stress for different cutout depth; (a) plate thickness equals 3mm, and (b) plate thickness equals 1mm

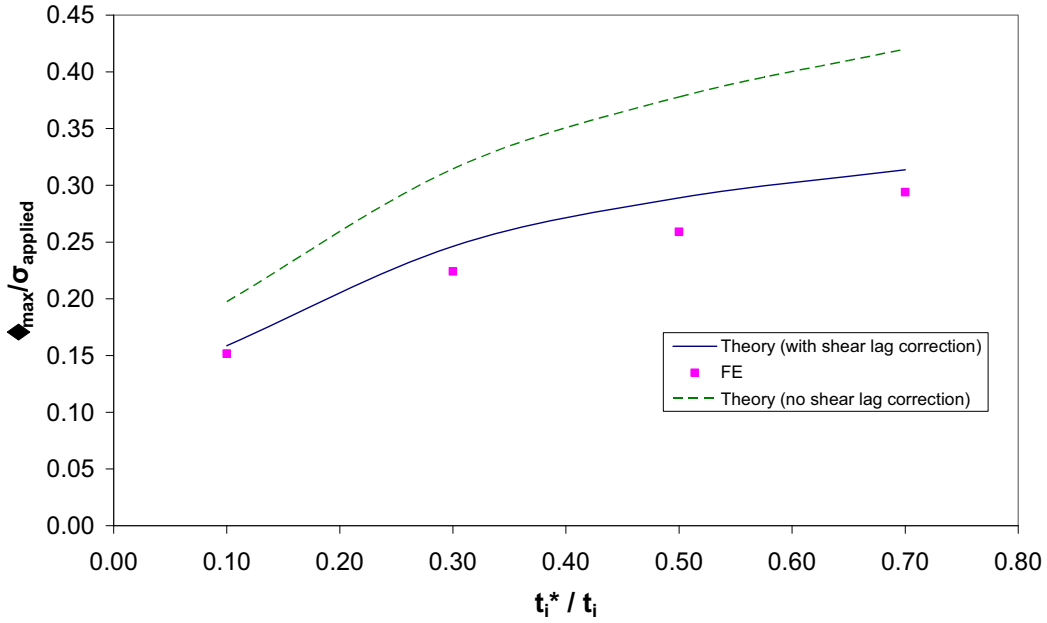

(a)

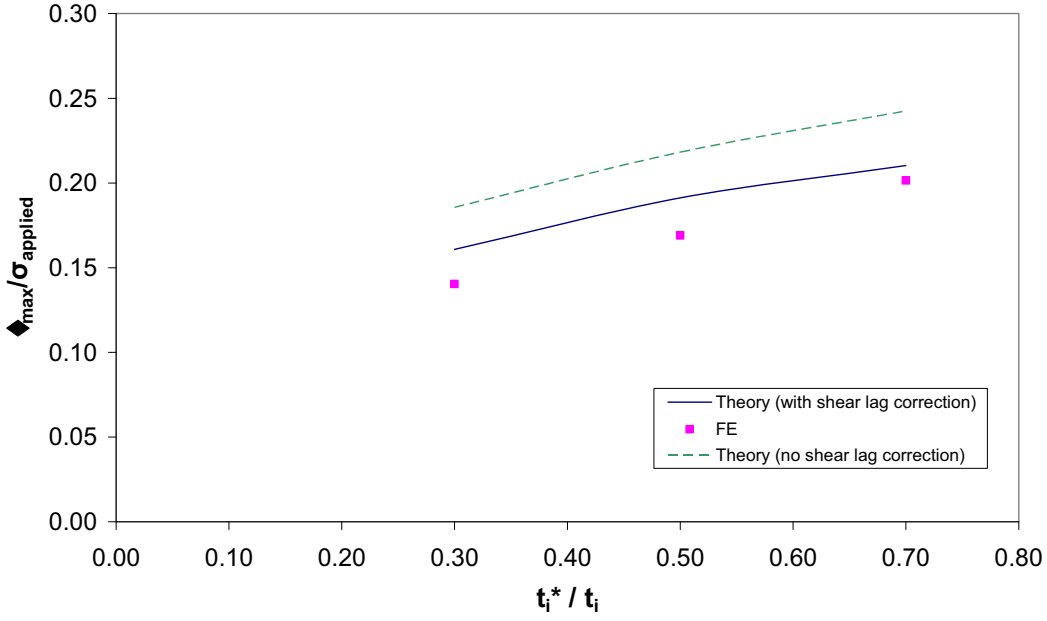

(b)

Figure 14: Maximum shear stress versus cutout depth; (a) plate thickness equals 3mm and (b) plate thickness equals 1mm

The existing repair design seeks to limit the maximum adhesive shear strain to remain below the adhesive's allowable strain, including plastic deformation. A comparison between the analytical estimate, expression (3), and the finite element results is presented in Figure 15. With the shear-lag correction, the analytical estimate of the applied stress for a given shear strain is conservative and within 20% of the finite element solution. Therefore the current analysis is considered to be satisfactory to serve as design tools.

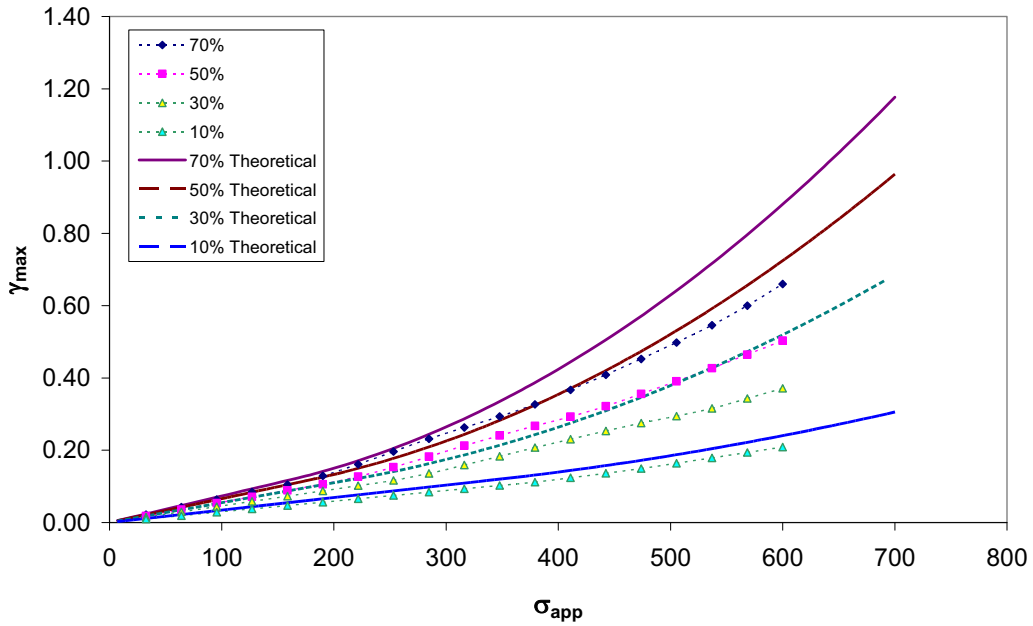

Figure 15: Maximum shear strain versus applied stress for straight-sided plug repair with the cutout being 10%, 30%, 50% and 70% of the parent thickness. Note Young's modulus used for the adhesive is 517 MPa.

5.4 Effect of Edge Tapering on Adhesive Stresses

Contour plots of the adhesive shear and peel stresses for the case of $t_e / t_o = 0.2$ are shown in Figure 16. The parent structure is subjected to a unit applied stress. It is clear that a corner singularity exists at the interface between repair and adhesive. However, the singularity field dominates only a very small distance around the corner and hence will not affect the mid-plane stresses in the adhesive.

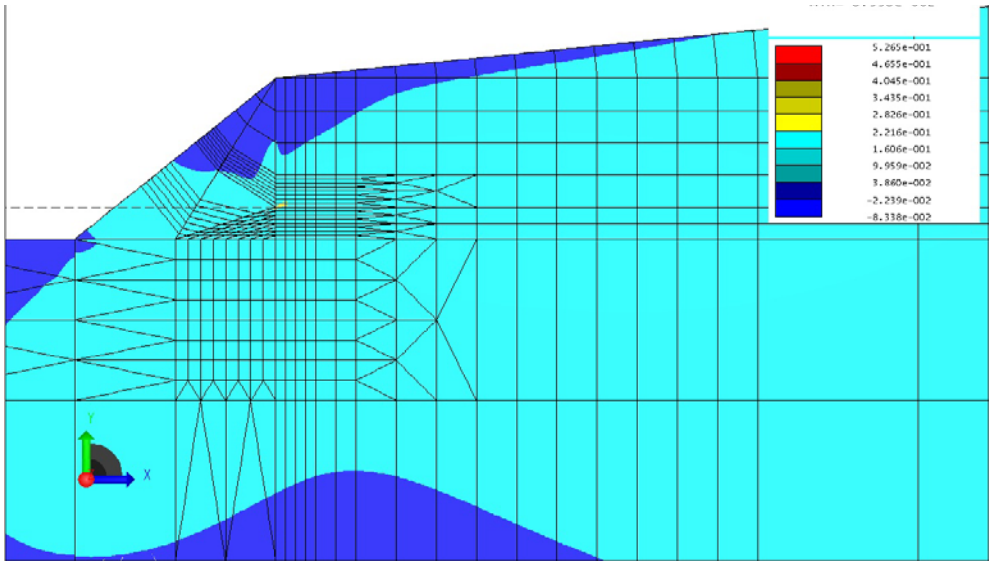

(a) Shear stress

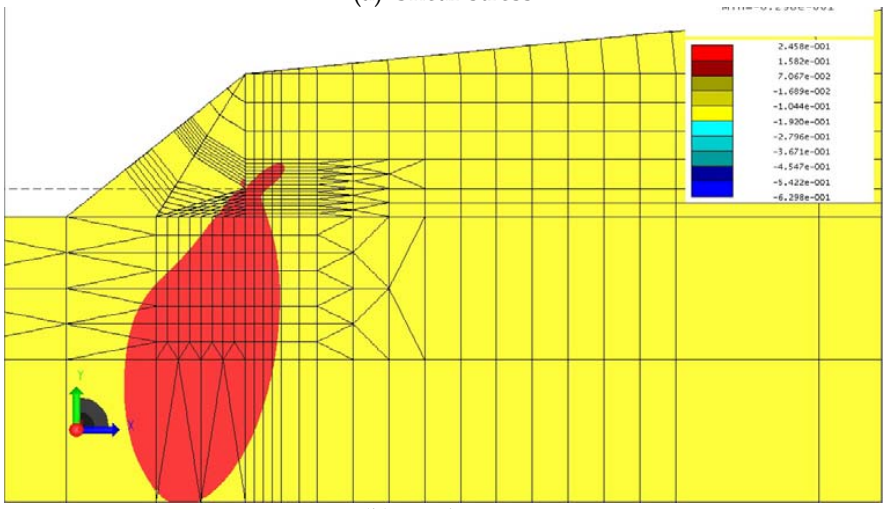

(b) Peel stress

Figure 16: Contours of (a) shear stress and (b) peel stress. Edge height is equal to 20% the full doubler thickness.

Results of the peel stress, normalised by the maximum peel stress pertinent to the uniform repair ($t_e = t_o$) are displayed in Figure 17. It is clear that the peel stress decreases with the edge height of the repair. The maximum peel stress is plotted against the ratio of edge height in Figure 18, indicating the current solution (6) overestimates the peel stress when the edge height is above 20% of the repair thickness. This would add to the level of conservatism in repair designs.

An improved solution, which also correctly recovers the results of uniform repair, is seen to provide a good correlation with the numerical results. The new solution is given by the following expression,

$$\frac{(\sigma_{c\max})_{tapered}}{(\sigma_{c\max})_{uniform}} = \sqrt{\frac{3t_e}{2t_e + t_o}}. \tag{7}$$

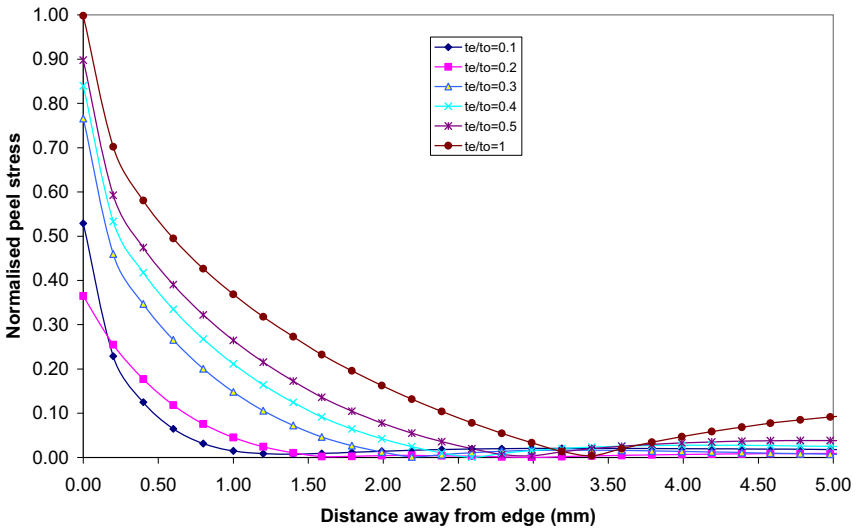

Figure 17: Distributions of normalised peel stress $\sigma_c/(\sigma_{c,\max})_{uniform}$ for varying edge heights

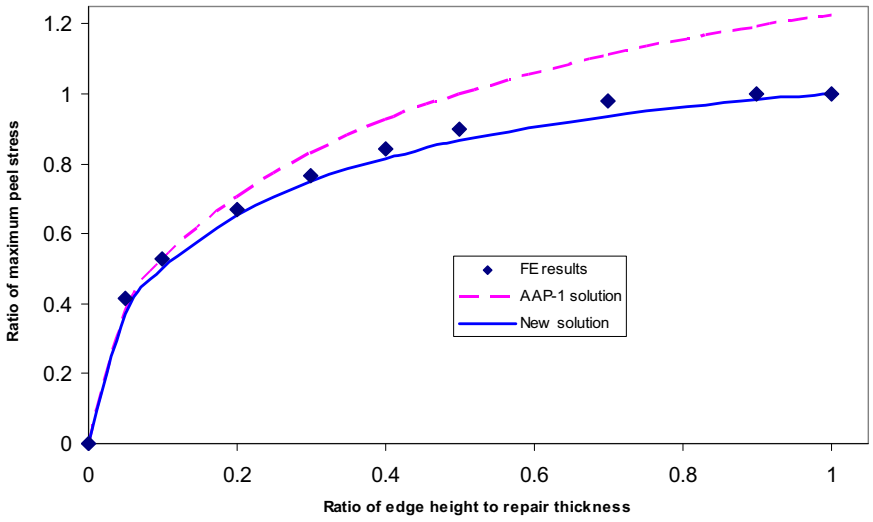

Figure 18: Ratio between the maximum peel stress at the edge of a tapered doubler to that pertinent to block-end doubler

6. Shear Lag Correction

The deformation behaviour of adherends is more complex than the assumed one-dimensional extension deformation by the beam-spring analysis. Because the through-thickness shear deformation of the adherends is not considered in the one-dimensional analysis, existing solutions tend to overestimate adhesive stresses. This effect is commonly refered to as the "shear-lag" effect [8]. For adherends made of isotropic materials, one shear-lag correction technique to lump the shear stiffness of the adherends together with the shear stiffness of the adhesive. In particular, a correction factor is applied to the load transfer parameter λ,

$$\lambda^2 = \frac{G\kappa}{\eta}\left(\frac{1-\nu_i^2}{E_i t_i} + \frac{1-\nu_o^2}{E_o t_o}\right), \tag{8}$$

with

$$\kappa = \frac{1}{1 + Gt_o/(3G_o\eta) + Gt_i/(3G_i\eta)}, \tag{9}$$

where G_i and G_o denote the shear moduli of the inner and outer adherends. A considerable improvement in the agreement between the analytical solution and the FE solution can be seen Figure 14. This will in turn reduce the level of conservatism of the current design method, enabling repairs of more highly loaded structures.

7. Required plastic zone size for repairs to part-through thickness defect

The plastic zone transfer lengths for repairs to part-through thickness defects, as illustrated in Figure 19, are given in Table 6-C3-4 of Ref [4]. These expressions ignore the load-carrying capacity of the unbroken ligament. As a result, the doubler length required for shallow corrosion damage would be excessively large.

An improved solution can be derived by accounting for the load being carried by the un-broken section of the structure. To be conservative, the load-carrying capacity of the insert plug is neglected. Furthermore, it is assumed that the cutout is optimally shaped such that the stress concentration factor in the unbroken ligament is approximately equal to unity. As shown in Figure 19, the design ultimate load (DUL) is shared between the unbroken ligament of the structure and the doubler. The load carried by the doubler is thus equal to

$$P_{doubler} = \frac{E_o t_o}{E_i (t_i - t_i^*) + E_o t_o} \mathrm{DUL}\,.$$

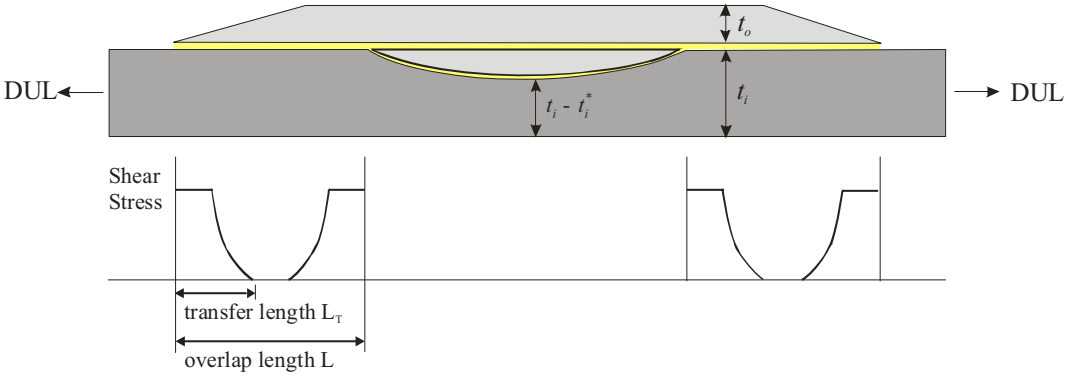

Figure 19: Load transfer in repair to part-through defect

This means that the area below the shear stress distribution outside the cutout region must equal the load carried by the doubler. This load equilibrium yields

$$2(l_p \tau_p + \frac{\tau_p}{\lambda}) = P_{doubler}\,. \tag{10}$$

Therefore the plastic zone transfer length l_p is

$$\begin{aligned} l_p &= \frac{E_o t_o}{E_i (t_i - t_i^*) + E_o t_o} \frac{\mathrm{DUL}}{2\tau_p} - \frac{1}{\lambda} \\ &\approx S \frac{\mathrm{DUL}}{2\tau_p} - \frac{1}{\lambda} \end{aligned} \tag{11}$$

where the equalities $E_o = E_i$ and $t_i^* = t_o$ have been used. The plastic zone transfer length would be zero if the elastic capacity exceeds the load to be carried by the doubler at ultimate design load. This can be expressed as

$$l_p = 0 \text{, if } \frac{1}{\lambda} > S\frac{\text{DUL}}{2\tau_p}. \tag{12}$$

The total transfer length then becomes

$$L_T = l_e + l_p = \begin{cases} S\dfrac{\text{DUL}}{2\tau_p} + \dfrac{2}{\lambda}, & \dfrac{1}{\lambda} \le S\dfrac{DUL}{2\tau_p} \\ \dfrac{3}{\lambda} & \dfrac{1}{\lambda} > S\dfrac{DUL}{2\tau_p} \end{cases}. \tag{13}$$

It is clear that for a grind out of shallow damage ($S << 1.0$), $l_p = 0$, and the total transfer length (basically the elastic transfer length) is considerably less than the expressions given in Table 6-C3-4 of Appendix 3 to Annex C, Chapter 6 [4].

8. Experimental Validation

To verify the design methodology for partial grind out repair, three representative repairs were performed on 2024-T3 aluminium alloy as shown in Figure 20. A part-depth grind out was machined into the aluminium structure, which is 6.35mm in thickness, to give a grind out depth of 50% the structure thickness. The grind outs were tapered at 90°, 30°, and 6°, respectively. The filler and the doubler, made of the same material, were bonded using FM300-2 film adhesive cured using the manufacturer's recommended process.

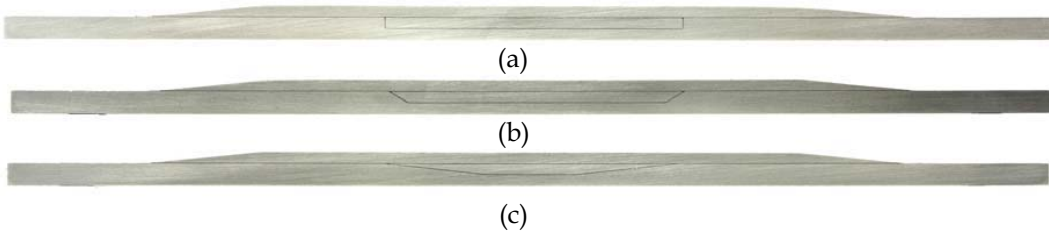

(a)

(b)

(c)

Figure 20: Repair joints to partial grind-out tapered at (a) 90°, (b) 30°, and (c) 6°

Specimens were loaded in tension, under displacement control, using a pin-loaded grip to minimise the bending. The presence of the external doubler introduces a load eccentricity that induces secondary bending. The eccentricity offset in load-path is equal to half the thickness of the doubler, i.e., 1.5mm. To further minimise the effect of secondary bending, two specimens were tested back-to-back. Typical examples of failure modes are presented in Figure 21. The experimental results, listed in Table 2, revealed that all three repairs reached a similar strength, with or without support against secondary bending. The overall bending of the specimens seen in Figure 21 was due to the plastic deformation of the cutout region, which experienced significantly higher stress after disbonding of the doubler.

(a) Un-supported against secondary bending

(b) Supported against secondary bending

Figure 21: Typical tension failures of repairs to part-through grind out: (a) un-supported against secondary bending, (b) supported

Table 2: Strength of partial grind out repair

Taper angle of cutout side (degrees)	Experimental strength (MPa)	Prediction (MPa)	
		Elastic adherends	Elastic-plastic adherends
6	375 (un-supported)	1500	420
	360 (supported)	1500	430
30	373 (un-supported)	368	368
90	385 (un-supported)	337	337

The experimental results listed in Table 2 confirmed that the secondary bending has a negligible effect on the repair strength. Owing to the relatively large length-to-thickness ratio of the repair coupons, the secondary bending effect is greatly relieved by the geometrically non-linear deformation. An example of the deformed geometry at an applied stress of 400 MPa is shown in Figure 22(a). As the applied stress increases, the neutral axis of the repaired region moves towards the load path, as seen in Figure 22(b), thus reducing the magnitude of the bending moment induced by the secondary bending. Linear elastic analysis suggested that the secondary bending ratio, defined as the ratio between the bending stress and the membrane stress, is equal to 1.0. Geometrically non-linear analysis, on the other hand, predicted the secondary bending ratio reduced to 0.13 as the applied stress increased to 400 MPa.

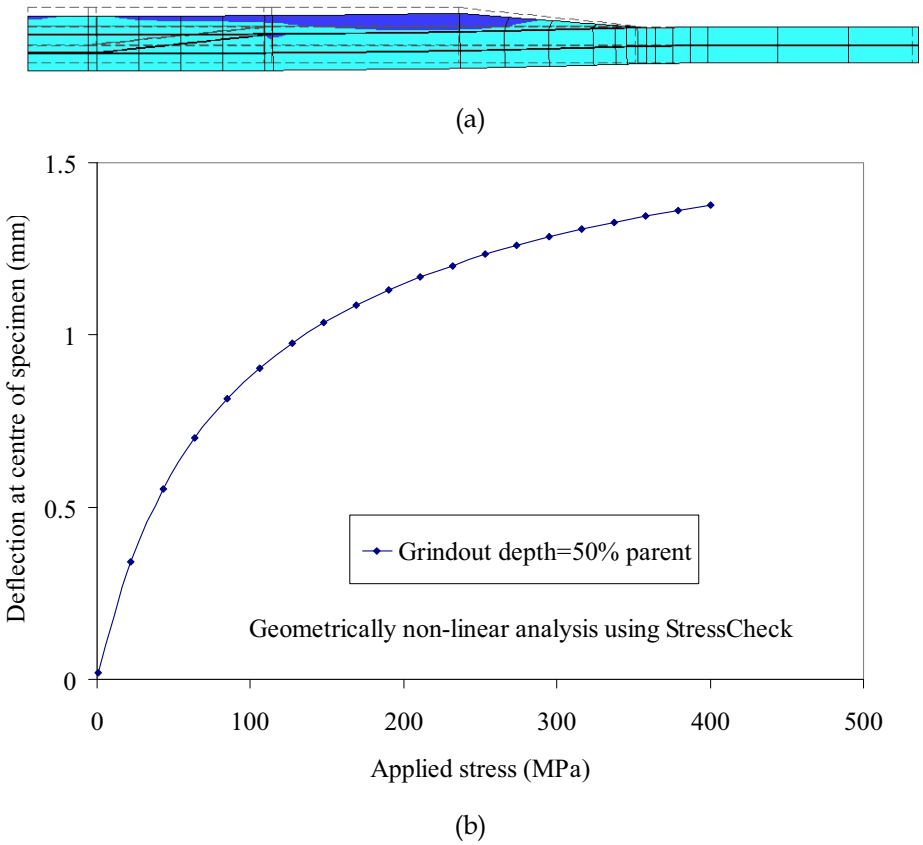

Figure 22: Geometrical non-linear deformation of repair under tension; (a) deformed geometry at any applied stress of 400 MPa, and (b) deflection at the centre of repair versus applied stress

The peak adhesive shear strain over the cutout region increases with the applied stress, as plotted in Figure 23. These results suggest that the 6°-cutout repair would have much higher bond strength than the repairs tapered at 30° and 90°, inconsistent with the experimental results. Detailed inspection of the failure processes revealed that disbonding of the doubler first occurred at the tapered ends, as shown in Figure 24.

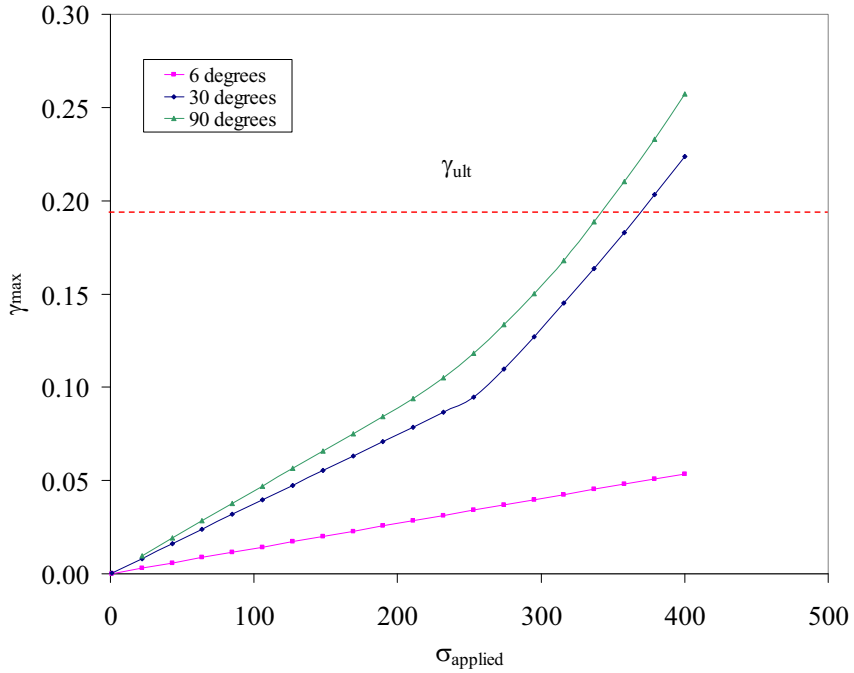

Figure 23: Maximum shear strains in the adhesive along the slope of the cutout

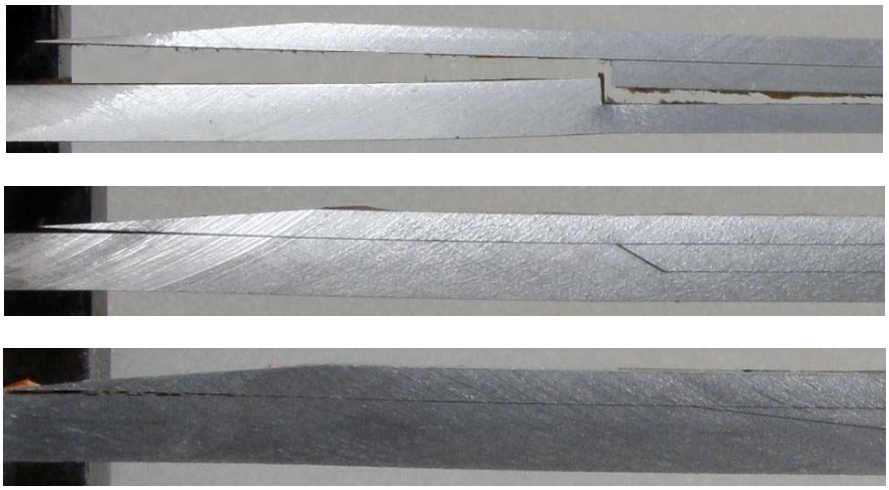

Figure 24: Disbonding of doubler at approximately 95% of the failure loads

The edge-disbonding observed in Figure 24 was the primary cause for failures of the repairs, as the filler would disbond instantly once the doubler peeled off. The maximum adhesive shear strain at the end of doubler was determined from the finite element analysis, assuming the aluminium adherends remain elastic. The results are presented in Figure 25. The FE results

indicate that the adhesive shear strain reaches the material failure strain of 0.19 at an applied stress of 550 MPa, which is significantly higher than the experimentally measured strength.

One possible reason for this over-prediction of strength was the plastic deformation of the aluminium adherend. Using the tensile stress-strain data of 2024-T3 aluminium alloy [9], the finite element analysis predicted a higher adhesive shear strain, as shown in Figure 25. According to the elastic-plastic analysis, doubler disbonding would occur at approximately 420 MPa, which is about 12% higher than the experimental strength. Further investigation of the doubler disbonding problem is needed to develop an improved tapering profile.

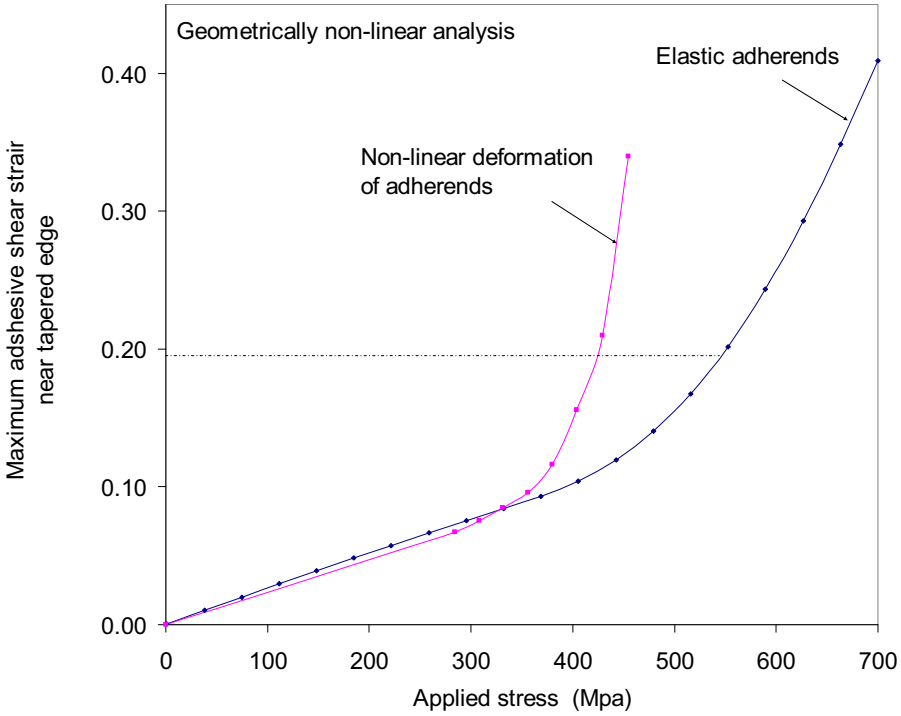

Figure 25: Maximum adhesive shear strain at the tip of the doubler

9. Conclusions

1. The design methodology recommended in AAP 7021.016-1 for plug-doubler repair to part-through defects has been computationally verified using the finite element method.
2. For moderately thick structures, e.g., thickness greater than 3 mm, it is important to incorporate the effect of shear lag in determining the adhesive stresses.
3. The sides of the cutout need to be tapered to an appropriate angle to avoid adhesive bond failure; the maximum allowable taper angle to achieve a given repair strength needs to be determined using the finite element method, as no closed-form solutions are currently available that account for the plastic deformation behaviour of adhesive.
4. The existing solution for the reduction in peel stress resulting from tapering the edge of repair has been found to be overly conservative. A new solution has been presented which is shown to agree well with finite element results.
5. An improved solution for the required overlap length has been developed. This new analysis takes into account the load-carrying capacity of the unbroken ligament, thus considerably reducing the unnecessary conservatism of the current methodology.

10. Recommendations

Results of the present investigation reveal the need to incorporate the following changes into RAAF's Composite and Adhesive Bonded Repair standard, AAP 7021.016-1.

1. Replace the peel stress solutions in Appendices 1-5, i.e., expressions (6.C.1.18), (6.C.2.18), (6.C.3.26), (6.C.4.16), (6.C.5.18), with the validated solution of (7).
2. Replace the plastic zone transfer allowance given in Table 6-C3-4 with the expression (11).
3. Incorporate a shear-lag correction to the shear-transfer parameter λ to account for the thickness effect of adherends. The correction factor is given by (9).
4. Slopes of the cutout must be tapered at an appropriate angle to be determined using detailed FE analysis to avoid bond failure.

11. Acknowledgements

The authors would like to acknowledge the assistance of Marilyn Anderson and Jack Singhavong with the experimental programme.

12. References

1. RAAF, *Composite and Adhesive Bonded Repairs Engineering and Design Procedures AAP 7021.016-1*. 2007, Royal Australian Air Force.
2. Rose, L.R.F. and C.H. Wang, *Analytical methods for designing composite repairs*, in *Advances in Bonded Composite Repairs of Metallic Aircraft Structure*, A.A. Baker, L.R.F. Rose, and R. Jones, Editors. 2002, Elsevier: Amsterdam. p. 137-175.
3. Duong, C.N. and C.H. Wang, *Composite repair: theory and design*. 2007, Oxford: Elsevier. 463.
4. RAAF, *Australian Air Publication AAP-7021.016-1 Repair Design Procedures*. 2006, RAAF.
5. RAAF, *DEF(AUST)9005 Issue A: Composite Materials and Adhesive Bonded Repairs*. 2005.
6. Wang, C.H., A.N. Rider, P. Chang, A. Charon, and A.A. Baker. *Structural repair techniques for highly-loaded carbon/BMI composites*. in *SAMPE Fall Technical Conference*. 2007. Cincinnati, OH, USA.
7. Callinan, R.J. and J.J. Paul, *Bonded repairs of metallic aircraft components damaged by corrosion*. 1993, Defence Science and Technology Organisation: Melbourne.
8. Chalkley, P.D. and L.R.F. Rose, *Variational bounds for the equivalent spring constants for bonded repairs*. 1998, Defence Science and Technology Organisation: Melbourne.
9. Handbook-5G1, M., *Metallic materials and elements for aerospace vehicle structures*. 1994, US Department of Defence.

DEFENCE SCIENCE AND TECHNOLOGY ORGANISATION
DOCUMENT CONTROL DATA

1. PRIVACY MARKING/CAVEAT (OF DOCUMENT)

2. TITLE

Design Methodology for Bonded Repair to Partial Through-Thickness Damage

3. SECURITY CLASSIFICATION (FOR UNCLASSIFIED REPORTS THAT ARE LIMITED RELEASE USE (L) NEXT TO DOCUMENT CLASSIFICATION)

Document (U)
Title (U)
Abstract (U)

4. AUTHOR(S)

Chun H. Wang and Dina Pilalias

5. CORPORATE AUTHOR

DSTO Defence Science and Technology Organisation
506 Lorimer St
Fishermans Bend Victoria 3207 Australia

6a. DSTO NUMBER	6b. AR NUMBER	6c. TYPE OF REPORT	7. DOCUMENT DATE
DSTO-TR-2117	AR- 014-166	Technical Report	September 2008

8. FILE NUMBER	9. TASK NUMBER	10. TASK SPONSOR	11. NO. OF PAGES	12. NO. OF REFERENCES
2008/1047839	AIR 07/053	DGTA	28	9

13. URL on the World Wide Web

http://www.dsto.defence.gov.au/corporate/reports/DSTO-TR-2117.pdf

14. RELEASE AUTHORITY

Chief, Air Vehicles Division

15. SECONDARY RELEASE STATEMENT OF THIS DOCUMENT

Approved for public release

OVERSEAS ENQUIRIES OUTSIDE STATED LIMITATIONS SHOULD BE REFERRED THROUGH DOCUMENT EXCHANGE, PO BOX 1500, EDINBURGH, SA 5111

16. DELIBERATE ANNOUNCEMENT

No Limitations

17. CITATION IN OTHER DOCUMENTS Yes

18. DSTO RESEARCH LIBRARY THESAURUS http://web-vic.dsto.defence.gov.au/workareas/library/resources/dsto_thesaurus.htm

Adhesive bonding, repair, composite structures, corrosion

19. ABSTRACT

Partial through-thickness damage to metallic and composite structures, like thosed caused by corrosion damage of metals or foreign object impact to composites, can be repaired by adhesively bonding an insert and an external doubler. The design methodology for these type of repairs is based on a simplified analyis in which the filler is assumed to be bonded to the flat bottom of the cutout area. This report presents a computational investigation of the accuracy and limitation of the curent design methodology. Based on the results of the finite element analysis an improved design methods are provided, including the optimum taper angle of damage grindout and the required overlap length.